International Core Journal of Engineering Volume 7 Issue 2, 2021
ISSN: 2414-1895 DOI: 10.6919/ICJE.202102_7(2).0026

Z-source Inverter of PV Ship Grid-connected Based on Robust Control

Yupan Fang[1,a], Shihong Gan[2,b], Weifeng Shi[2,c]

[1]Merchant Marine College of Shanghai Maritime University, Shanghai 200000, China;

[2]Electrical Department of Shanghai Maritime University, Shanghai 200000, China.

[a]3056556899@qq.com, [b]shgan@shmtu.edu.cn, [c]fewei@shumtu.edu.cn

Abstract

Applying photovoltaic power generation system to the ship's power grid will reduce the pollution of ship to the ocean. In order to improve the efficiency and quality of photovoltaic power generation on board the ship, In this paper, robust control is used in DC side, and Z-source capacitor voltage outer loop control and current inner loop control are used in AC side, The robust controller and regulator are designed to realize the fast tracking of grid-connected current. At the same time, active damping technology is also used on the grid side to suppress the resonance of the LCL filter, which improves the reliability of the ship grid-connected system. Finally, simulations verify the correctness and effectiveness of the theory.

Keywords

Grid Structure; Z-Source Inverter; PV Grid-Connected; Robust Control; PI Algorithm.

1. Introduction

With the rapid development of the world economy, the non-renewable energy that promotes the development of the world economy is facing exhaustion. Ships are important means of transportation for the development of the world's maritime economy. In order to improve the energy structure of ships, this article applies photovoltaic power generation to the ship’s power grid, which will reduce the ship’s consumption of non-renewable energy.

In order to further improve the efficiency of photovoltaic power generation, this paper applies the Z-source inverter proposed by Professor Peng Fangzheng to the ship, and the Z-source inverter has been deeply studied in references [1 - 2]. Aiming at the grid-connected control, the robust control is designed in this paper, and the stable grid connected current waveform is obtained, which effectively suppresses the shortcomings of traditional inverter such as large grid-connected harmonics.

2. Photovoltaic ship power grid system

2.1 Photovoltaic ship power grid system structure

The structure of the connection between the solar panel and the ship's power grid is shown in Fig. 1. The leftmost part of the figure is the solar panel, $ACB_1 - ACB_3$ and $MCB_1 - MCB_7$ for various switches, $MSB, DSB, ISB, IDSB$ for the distribution board. G_1, G_2 is diesel generator set, SC is shore power box, M_1, M_2 is the load motor on board, T_r is lighting transformer.

After inverter inversion, the solar panel is connected to the main distribution board of the ship power grid. Both the generator and the solar panel are the power supply equipment of the ship. When the weather is sunny, the solar energy can provide power for the ship power grid, which can reduce the number and capacity of the marine diesel generator set.

ISSN: 2414-1895 DOI: 10.6919/ICJE.202102_7(2).0026

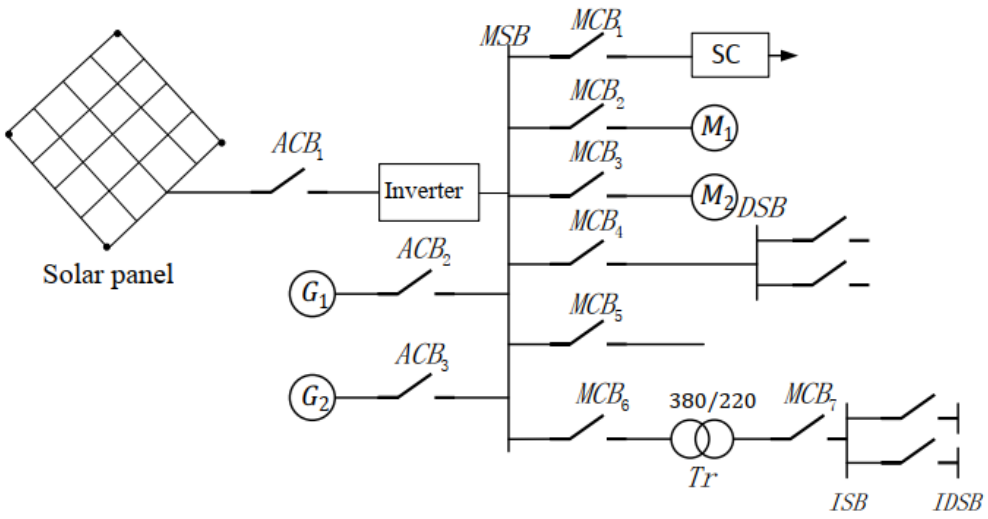

Fig. 1 Ship power grid system structure

2.2 Z-source photovoltaic grid-connected inverter system

LCL filter Z-source photovoltaic grid-connected inverter system is shown in Fig. 2. In the figure, i_{PV} is the output current of solar panel, i_{pv} is the flow through C_{pv} current, i_{D_1} is diode D_1 current, **K** is robust controller, M is Z-source inverter modulation factor, D_0 is the shoot-through duty cycle of Z-source inverter.

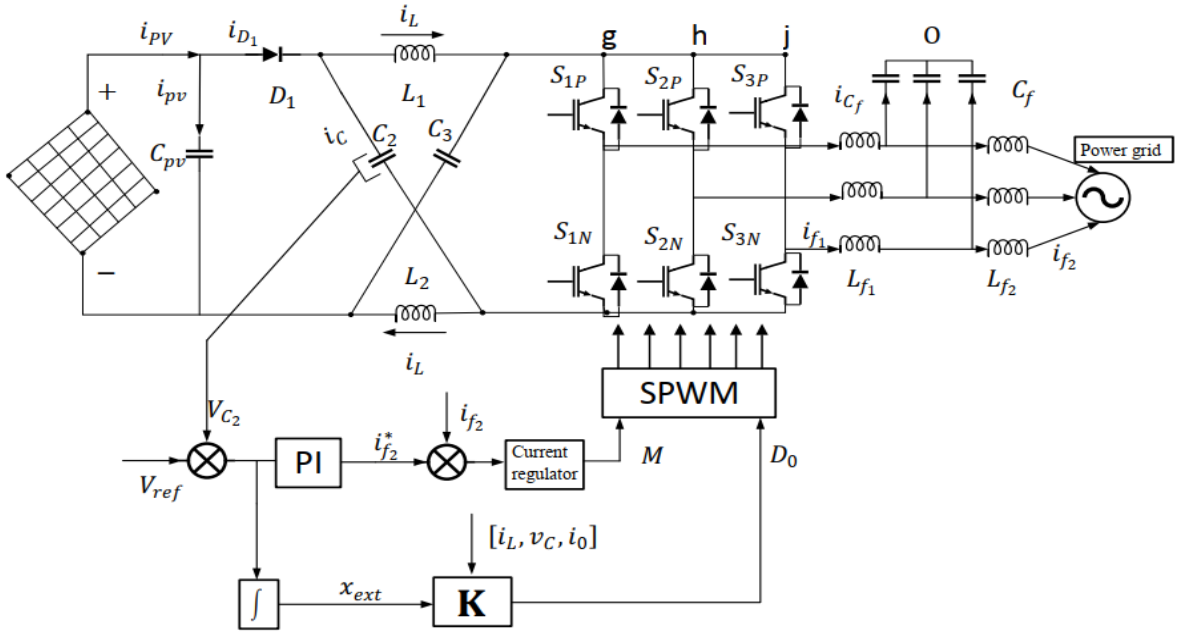

Fig. 2 Z-source PV grid-connected inverter system

In Fig. 2, assuming that the circuit is symmetrical, that is $C_2 = C_3 = C$, $L_1 = L_2 = L$,then $V_{L_1} = V_{L_2} = V_L$, $V_{C_2} = V_{C_3} = V_C$. The Z-source inverter has two modes of shoot-through and non-shoot-through .In the shoot-through mode, the circuit is shown in Fig. 3(a), and equation (1) can be obtained:

$$\begin{cases} V_L = V_C \\ V_i = 0 \end{cases} \tag{1}$$

In the non-shoot-through mode, the circuit is shown in Fig. 3(b), and equation (2) can be obtained:

$$\begin{cases} V_L = V_{pv} - V_C \\ V_i = V_C - V_L \end{cases} \tag{2}$$

ISSN: 2414-1895 DOI: 10.6919/ICJE.202102_7(2).0026

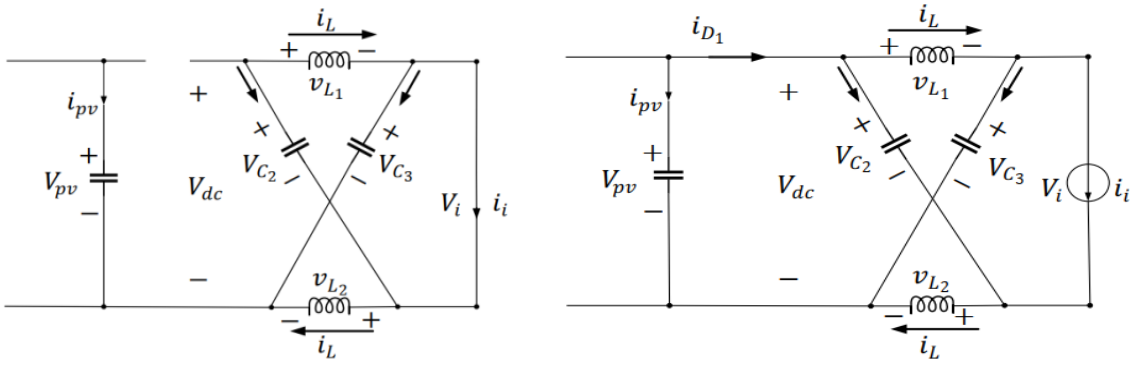

a. shoot-through mode b. non-shoot-through mode

Fig. 3 Equivalent circuit of Z-source inverter

In steady state, the average inductor voltage in a cycle is 0, so

$$V_C D_0 T + (V_{pv} - V_C)(1 - D_0)T = 0 \tag{3}$$

Where, T is switching period; T_0 is shoot-through time; $D_0 = {}^{T_0}/_{T}$, D_0 is shoot-through duty cycle;(4) can be obtained by equation (3)

$$V_C = \frac{1 - D_0}{1 - 2D_0} V_{pv} \tag{4}$$

The peak value of DC link voltage is:

$$V_i = \frac{1}{1 - 2D_0} V_{pv} = BV_{pv} \tag{5}$$

Where, B is the boost factor, so the output voltage peak value of grid-connected inverter can be expressed as:

$$v_{in} = \frac{BMV_{pv}}{2} \tag{6}$$

According to equation (6), the output voltage of the inverter can be determined by B and M. Compared with the traditional inverter, the output voltage range of the inverter is further expanded.

3. Mathematical model of Z-source PV grid-connected system

3.1 Mathematical model of Z-source inverter circuit

As shown in Fig. 3, if the capacitor voltage and inductance current are taken as state variables, the state equation of the shoot-through mode is as follows:

$$\begin{bmatrix} \frac{di_L}{dt} \\ \frac{dv_C}{dt} \end{bmatrix} = \begin{bmatrix} 0 & \frac{1}{L} \\ -\frac{1}{C} & 0 \end{bmatrix} \begin{bmatrix} i_L \\ v_C \end{bmatrix} \tag{7}$$

The state equation of non-shoot-through mode is as follows:

$$\begin{bmatrix} \frac{di_L}{dt} \\ \frac{dv_C}{dt} \end{bmatrix} = \begin{bmatrix} 0 & -\frac{1}{L} \\ \frac{1}{C} & 0 \end{bmatrix} \begin{bmatrix} i_L \\ v_C \end{bmatrix} + \begin{bmatrix} \frac{v_{pv}}{L} \\ -\frac{i_i}{C} \end{bmatrix} \tag{8}$$

From equations (7) and (8), the average state equation of the Z-source network is:

$$\begin{bmatrix} \frac{di_L}{dt} \\ \frac{dv_C}{dt} \end{bmatrix} = \begin{bmatrix} 0 & \frac{2D_0 - 1}{L} \\ \frac{1 - 2D_0}{C} & 0 \end{bmatrix} \begin{bmatrix} i_L \\ v_C \end{bmatrix} + \begin{bmatrix} \frac{(1 - D_0)v_{pv}}{L} \\ \frac{(D_0 - 1)i_i}{C} \end{bmatrix} \tag{9}$$

ISSN: 2414-1895 DOI: 10.6919/ICJE.202102_7(2).0026

3.2 Mathematical model of grid-connected inverter

If the loss is ignored, the input DC power of the inverter bridge is equal to the output AC power of the inverter bridge:

$$V_i I_i = \frac{\sqrt{3} E_g I_{f\,2}}{2} \tag{10}$$

Where V_i is bus voltage of inverter bridge in non-shoot-through mode, I_i is average current of DC bus in non-shoot-through mode, E_g is peak value of EMF, I_{f2} is peak value of grid-connected current. Available

$$I_i = \frac{\sqrt{3} E_g I_{f\,2}}{2V_i} \tag{11}$$

In the shoot-through model, equation (12) can be obtained from Fig. 3.

$$I_i = 2I_L \tag{12}$$

The average value of DC bus current in a cycle is:

$$I = 2D_0 I_L + (1 - D_0)\frac{\sqrt{3} E_g I_{f\,2}}{2V_i} \tag{13}$$

From equation (13) and fig. 3 (b), it is concluded that:

$$V_C(s) = \frac{(1 - 2D_0) I_L - (1 - D_0)\frac{\sqrt{3} E_g I_{f\,2}}{2V_{i_2}}}{Cs} \tag{14}$$

4. Grid-connected control strategy of Z-source PV inverter

4.1 Control strategy of AC side inverter

Z-source PV grid-connected includes DC boost control and AC inverter control. The system has a large amplitude at the resonance frequency and a small system damping coefficient. If it is not controlled, it will produce a lot of harmonics. In this paper, active damping is used to reduce the pollution of harmonics to the power grid. Fig. 4 is the LCL filter capacitor current virtual resistance R feedback active damping block diagram, where v_{in} is the output voltage of the inverter.

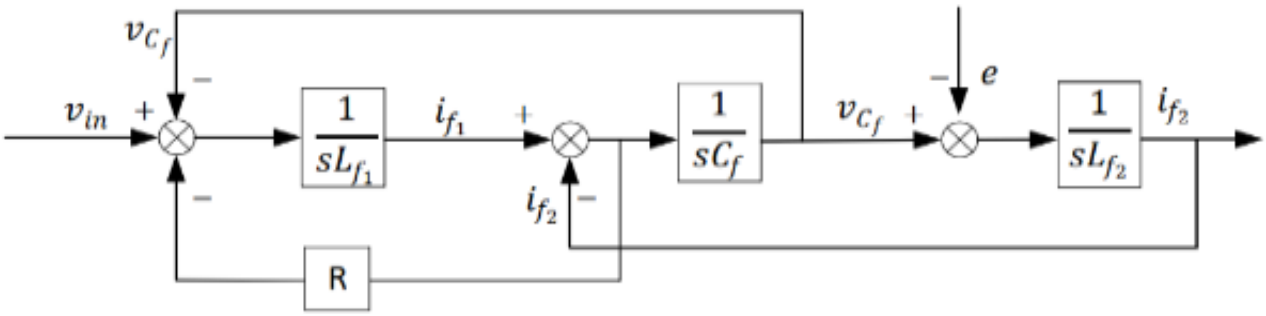

Fig. 4 Block diagram of active damping LCL filter

Equation (15) can be obtained:

$$i_{f_2} = \frac{1}{s^3 L_{f_1} L_{f_2} C_f + s^2 L_{f_2} C_f R + s(L_{f_1} + L_{f_2})} v_{in} - \frac{s^2 L_{f_1} C_f + s C_f R + 1}{s^3 L_{f_1} L_{f_2} C_f + s^2 L_{f_2} C_f R + s(L_{f_1} + L_{f_2})} e \tag{15}$$

Fig. 5 shows Bode figure of transfer function of grid connected current i_{f_2} to input voltage v_{in} of inverter

ISSN: 2414-1895 DOI: 10.6919/ICJE.202102_7(2).0026

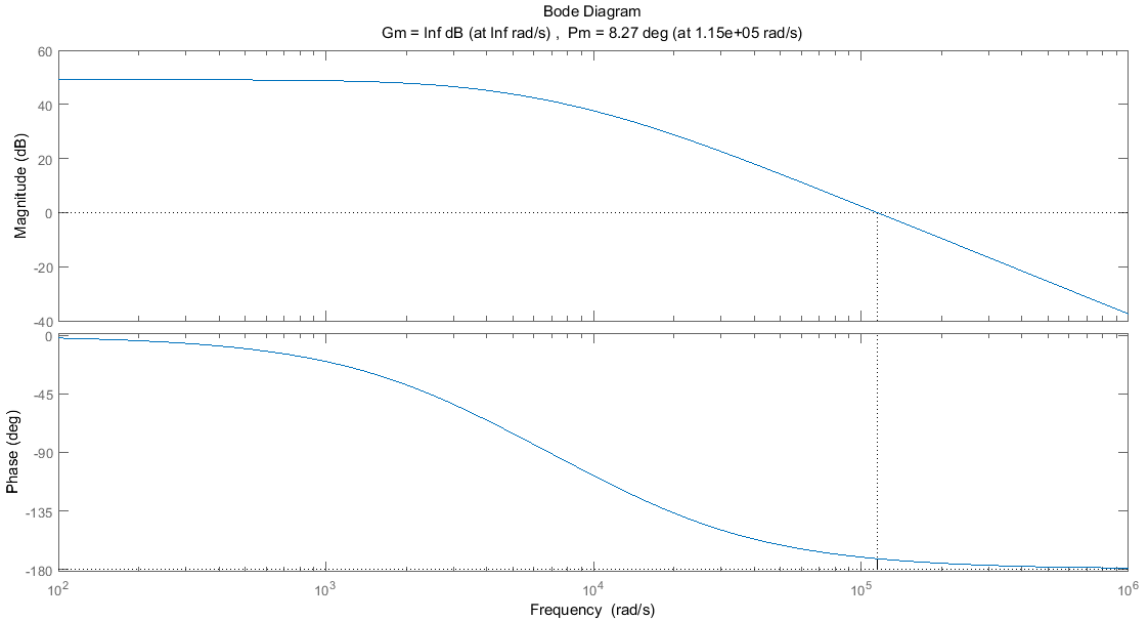

Fig. 5 Bode figure

In order to simplify the open-loop transfer function of grid-connected current at AC side, the LCL transfer function of the filter can be simplified as equation (16)

$$i_{f_2} = \frac{1}{Ls + R} v_{in} \tag{16}$$

Where $\mathrm{L} = L_{f_1} + L_{f_2}$、R is virtual resistance.

As shown in Fig. 6, it is the control block diagram of AC side grid-connected. The simplified function of the filter is used in the figure, where K_{PWM} is the magnification of the inverter; $\mathrm{T_s}$ is the sampling period; $\mathrm{T_{sw}}$ is the PWM switching period; $i_{f_2}^*$ is the given value of grid-connected current, which is obtained by PI adjustment of the error between the measured value of Z source capacitance and the given value, as shown in Fig. 2. In order to realize the fast and accurate tracking of grid-connected current, the current regulator is realized by proportional integral. Fig. 7 can be obtained by calculation and equivalent simplification of Fig. 6. From Fig. 7, the open-loop transfer function of the AC side grid-connected can be deduced as:

$$G_{crt} = \frac{(sK_{pcrt} + K_{icrt})K_{pwm}}{(1.5T_s + 0.5T_{sw})Ls^3 + (1.5T_sR + 0.5T_{sw}R + L)s^2 + Rs} \tag{17}$$

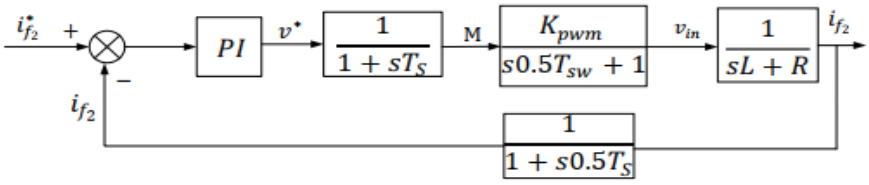

Fig. 6 Block diagram of AC side grid-connected control

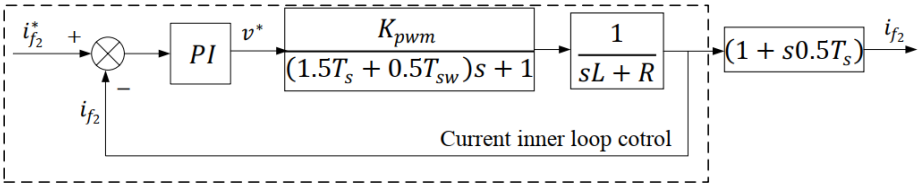

Fig.7 simplified grid-connected control block diagram

ISSN: 2414-1895 DOI: 10.6919/ICJE.202102_7(2).0026

4.2 DC side inverter boost control strategy

The linear matrix inequality (LMI) robust control method is adopted. Fig. 8 is the robust controller figure, w is the load disturbance output current I_{dis}, u is the shoot-through duty cycle d, K is the robust state feedback controller, x is the state variables, namely i_L, v_C and i_i. z is the output Z-source capacitor voltage.

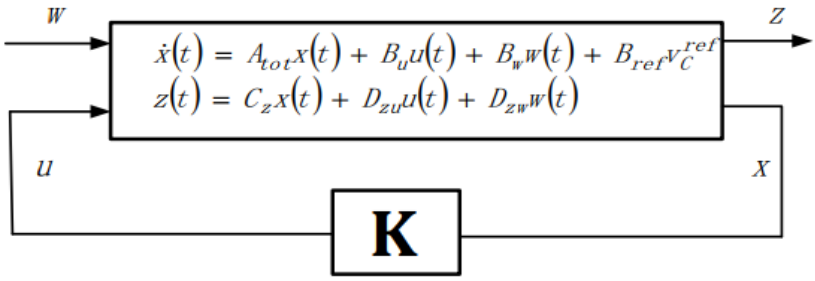

Fig. 8 robust controller

The whole system can be equivalent to equation (18)

$$\begin{cases} \dot{x}(t) = A_{tot}x(t) + B_u u(t) + B_w w(t) + B_{ref} v_C^{ref} \\ z(t) = C_Z x(t) + D_{zu} u(t) + D_{zw} w(t) \end{cases} \tag{18}$$

where $C_z = [0 \quad 1 \quad 0 \quad 0]$, $D_{zu} = 0$, $D_{zw} = 0$, $w(t) = I_{dis}(t)$, $u(t) = d$. The grid-connected side is equivalent to the combination of resistance and inductance, and the circuit in shoot-through and non-shoot-through state is equivalent to Fig 9.

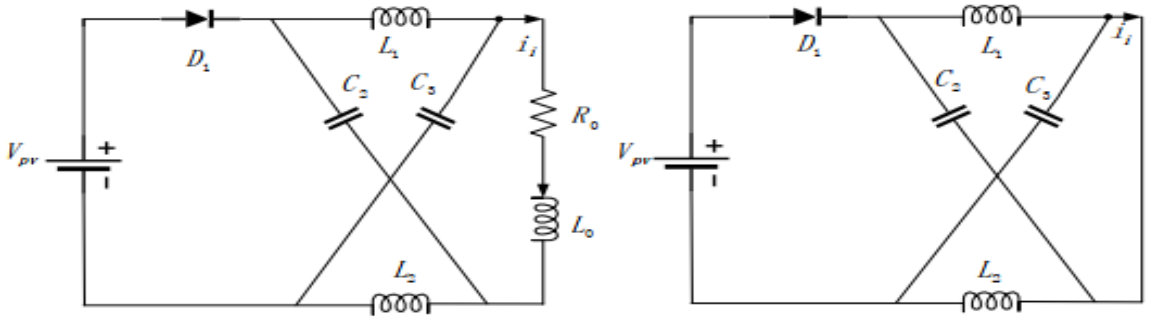

a) non-shoot-through equivalent circuit b) shoot-through equivalent circuit

Fig. 9 Equivalent circuit

Using the state space averaging method and small signal model processing, the parameter matrix (19) - (22) is derived:

$$A_{tot} = \begin{bmatrix} 0 & \frac{2D_0 - 1}{L} & 0 & 0 \\ -\frac{2D_0 - 1}{C} & 0 & -\frac{1 - D_0}{C} & 0 \\ 0 & \frac{2(1 - D_0)}{L_0} & -\frac{R_0}{L_0} & 0 \\ 0 & -1 & 0 & 0 \end{bmatrix} \tag{19}$$

ISSN: 2414-1895 DOI: 10.6919/ICJE.202102_7(2).0026

$$B_u = \begin{bmatrix} \frac{2V_C - V_{pv}}{L} \\ \frac{I_i - 2I_L}{C} \\ \frac{2V_C - V_{pv}}{L_0} \\ 0 \end{bmatrix} \tag{20}$$

$$BW = \begin{bmatrix} 0 \\ -\frac{1 - D_0}{C} \\ 0 \\ 0 \end{bmatrix} \tag{21}$$

$$B_{ref} = \begin{bmatrix} 0 \\ 0 \\ 0 \\ 1 \end{bmatrix} \tag{22}$$

Where, R_0 is the equivalent load, L_0 is the equivalent inductance, and v_{pv} is the input DC voltage of the Z-source network. There are uncertain parameters in the control system shoot-through duty cycle D_0 and load R_0, but the ranges of the two are $[D_{0\min}, D_{0\max}]$ and $[R_{0\min}, R_{0\max}]$. Both A_{tot} and B_u are affected by these parameters. In the design process, the following theorems were used:

Quadratic stability linear matrix inequality (LMI) Theorem: If the state feedback controller $u = \mathbf{K}x$ and $\mathbf{K} = YW^{-1}$ can make the system represented by equation (18) stable, then if and only if the symmetric matrix W and matrix Y satisfy the inequality:

$$\begin{cases} W > 0 \\ A_{tot}W + WA_{tot}^T + B_uY + Y^TB_u^T < 0 \end{cases} \tag{23}$$

H_∞ control linear matrix inequality theorem: If there are symmetric positive definite matrix W and matrix Y satisfying inequality (24), the state feedback controller $u = \mathbf{K}x$ and $\mathbf{K} = YW^{-1}$ can make the system represented by equation (18) satisfy $\|T_{zw}\|_\infty < \gamma$, thereby ensuring the minimum disturbance interference level.

$$\begin{bmatrix} A_{tot}W + WA_{tot}^T + B_uY + Y^TB_u^T & B_w & WC_y^T + Y^TD_{yu}^T \\ B_w^T & -\gamma^1 & 0 \\ C_yW + D_{yu}Y & 0 & -\gamma^1 \end{bmatrix} < 0 \tag{24}$$

Pole configuration linear matrix inequality theorem: If there are symmetric positive definite matrix W and matrix Y satisfying inequality (25)-(27), the state feedback controller $u = \mathbf{K}x$ and $\mathbf{K} = YW^{-1}$ can locate the closed-loop poles of the system represented by equation (18) in the area shown in Fig. 10.

ISSN: 2414-1895 DOI: 10.6919/ICJE.202102_7(2).0026

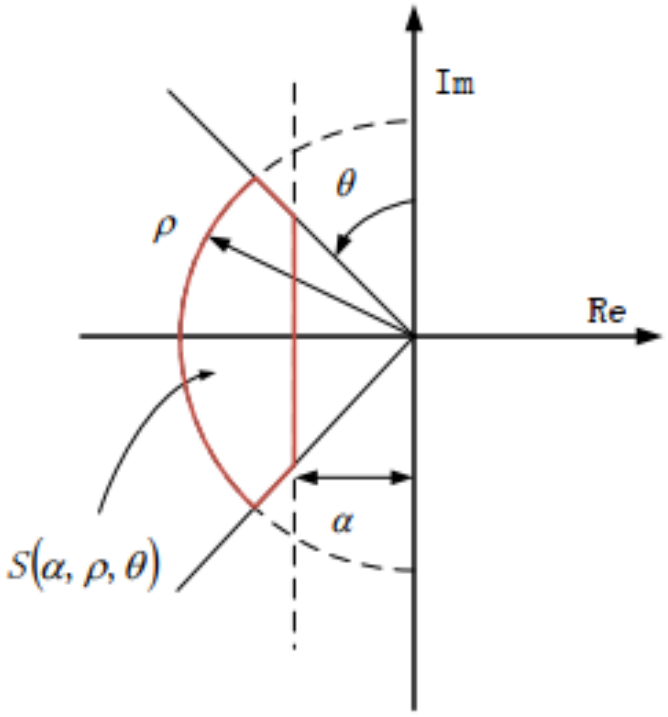

Fig.10 Zero and pole configuration area

With the help of Matlab, the robust state feedback controller K is calculated. Assuming $\mathrm{K} = \begin{bmatrix} k_2 & k_2 & k_3 & k_4 \end{bmatrix}$, the shoot-through duty cycle is $d(t) = k_1 i_L + k_2 v_C + k_3 i_i + k_4 x_{ext}$.

$$A_{tot}W + WA_{tot}^T + B_u Y + Y^T B_u^T + 2\alpha W < 0 \tag{25}$$

$$\begin{bmatrix} -\rho W & WA_{tot}^T + Y^T B_u^T \\ AW + B_u Y & -\rho W \end{bmatrix} < 0 \tag{26}$$

$$\begin{bmatrix} \cos\theta\left(A_{tot}W + WA_{tot}^T + B_u Y + Y^T B_u^T\right) & \sin\theta\left(A_{tot}W - WA_{tot}^T + B_u Y - Y^T B_u^T\right) \\ \sin\theta\left(-A_{tot}W + WA_{tot}^T - B_u Y + Y^T B_u^T\right) & \cos\theta\left(A_{tot}W + WA_{tot}^T + B_u Y + Y^T B_u^T\right) \end{bmatrix} < 0 \tag{27}$$

5. Simulations

In order to verify the feasibility of the above theory, this paper uses Matlab/simulink software to establish a simulation model of the Z-source ship PV grid-connected inverter. Take the Z-source network parameters $\mathrm{L_1} = \mathrm{L_2} = \mathrm{L} = 5\mathrm{mH}$, $\mathrm{C_2} = \mathrm{C_3} = \mathrm{C} = 1000\mu\mathrm{F}$, the filter LCL parameters $L_{f_1} = 4mH$, $L_{f_2} = 0.5mH$, $C_f = 130\mu F$, and the switching frequency is $10\mathrm{kH_Z}$.

The robust controller is calculated as $\mathrm{K} = \begin{bmatrix} -0.085 & -0.0072 & 0.0322 & 1.5645 \end{bmatrix}$. When $V_{pv} = 200V$, $D_0 = 0.22, \mathrm{M} = 0.86$, the voltage outer loop control PI is $K_{pVc} = 0.68, K_{iVc} = 15.3$. The current inner loop control regulator value is $K_{pcrt} = 39, K_{icrt} = 0.00000275$. The sum of LCL inductor resistance is r = 40. From equations (4)-(6), we can get: $V_C = 280V, V_i = 360V, v_{in} = 310V$. The simulation results are shown in Fig. 11, where Fig. 11a is the simulation curve of the Z-source grid-connected inverter under robust control + PI control. It can be seen that when V_{pv} gradually rises from 0 to 200V, V_C、V_i and i_L stabilize at 279.5V, 359.6V and 3A respectively after a brief fluctuation, and their values are consistent with theoretical calculations.

ISSN: 2414-1895 DOI: 10.6919/ICJE.202102_7(2).0026

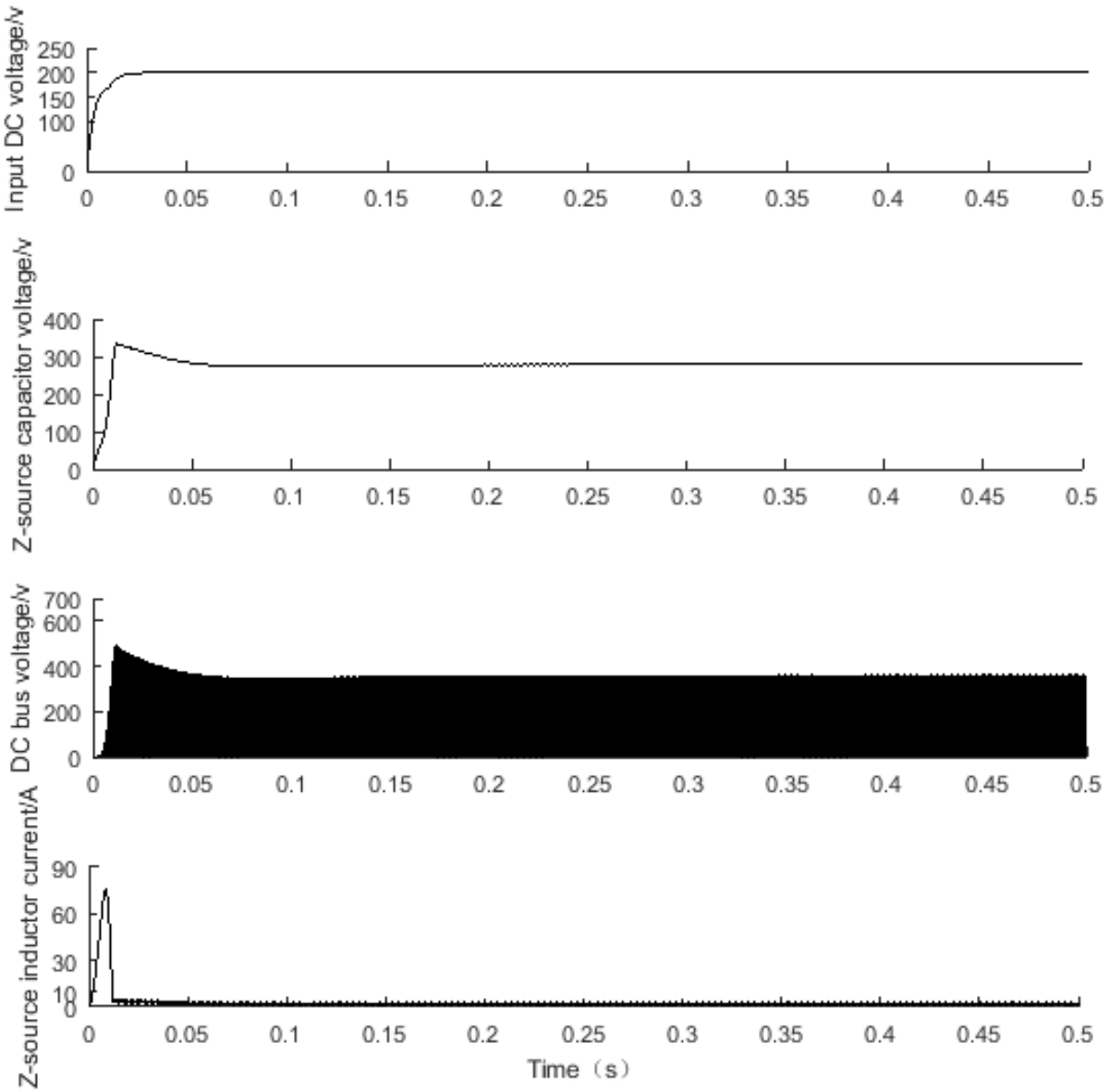

a. z source inverter

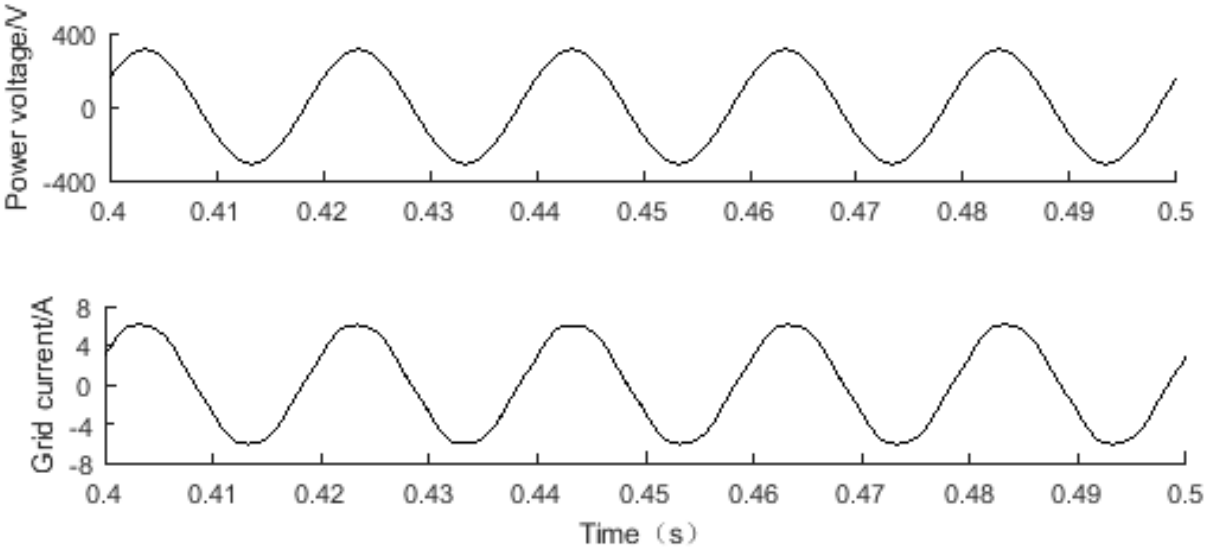

b. A-phase grid-connected current curve

Fig.11 Simulation results

ISSN: 2414-1895 DOI: 10.6919/ICJE.202102_7(2).0026

Fig. 11 b shows the steady-state curve of A-phase grid-connected current. It can be seen that the grid-connected current waveform and the grid waveform are sine waves that maintain the same frequency, and resonance is effectively suppressed.

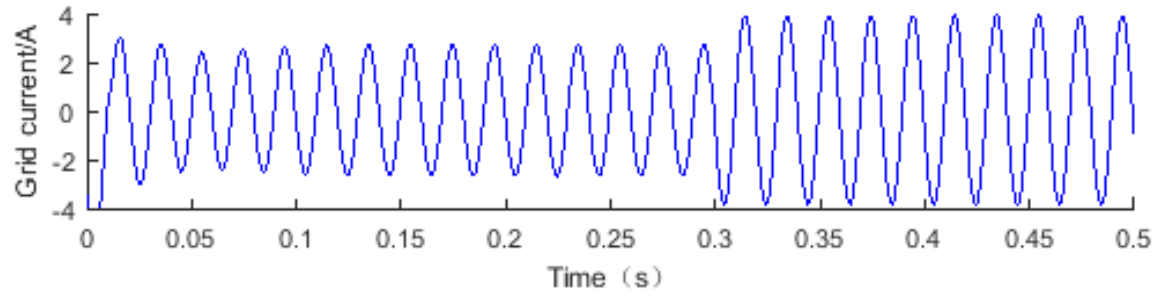

a. Grid current

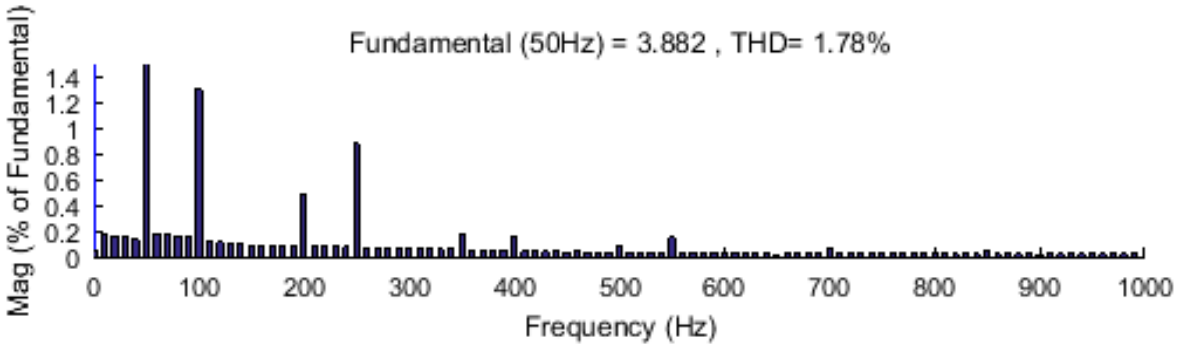

b. THD analysis

Fig. 12 Grid-connected current analysis under load changes

Fig. 12a is the waveform figure of the grid-connected current when the load changes suddenly at t = 0.3s, and the corresponding grid-connected current THD analysis result is shown in Fig. 12b. It can be seen from the figure that under the robust control + PI control, when the load changes, the grid-connected current can be stabilized within a cycle, there is no obvious overshoot. And only 1.78% in the THD analysis, making the grid current harmonics less.

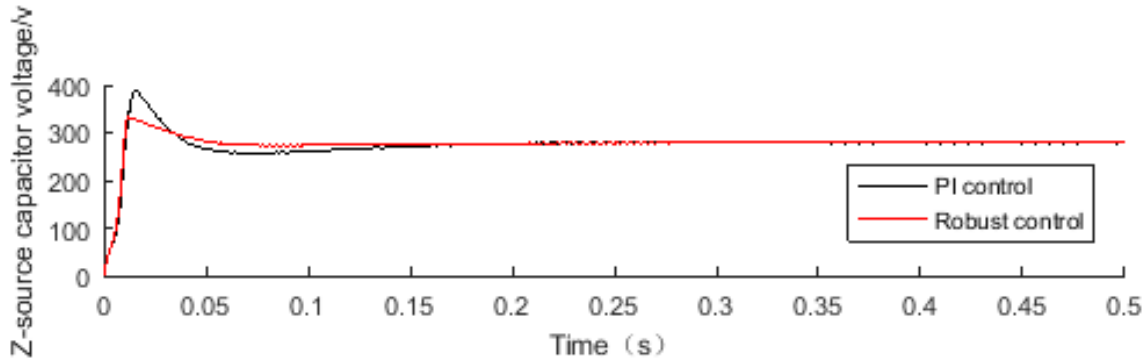

Fig. 13 V_C waveform under $D_0 = 0.22$

Fig. 13 is a waveform figure of the Z-source capacitor voltage V_C with robust control and PI control on the DC side when $D_0 = 0.22$. It can be seen from the figure. that robust control has many advantages over PI control under the same conditions, such as The fluctuation range is small and stable fast.

ISSN: 2414-1895 DOI: 10.6919/ICJE.202102_7(2).0026

6. Conclusion

In this paper, photovoltaic power generation is applied to ships, which effectively reduces the emission of harmful gases from ships; the use of active damping LCL filters on the power grid side suppresses the pollution of harmonics to the power grid. Robust control and PI control are used in the control to ensure the stability of grid-connected current when external conditions change, and improve the reliability of grid-connected. Finally, the validity of this theory is verified by simulation.

Acknowledgments

This work was supported by Shanghai Science and Technology Commission project (Grant No. 20040501200, 19040501700,)

References

[1] M.C. Cavalcanti, F. Bradaschia, M.T. de Melo Neto, G. Azevedo, T.D. Cardoso,Dynamic modeling and control system design of the buck-boost-based three-state three-phase Z-source inverter, Int. J. Electric. Power Energy Syst. 104 (2019) 654–663.

[2] Y. Huang, M.Shen, F.Z.Peng,J. Wang, Z-source inverter for residential photovoltaic systems, IEEE Trans. Power Electron. 21 (6) (2006) 1776–1782.

[3] Ali Rıza Yılmaz, Bilal Erol, Akın Delibaşı, et al. Design of gain-scheduling PID controllers for Z-source inverter using iterative reduction-based heuristic algorithms.Simulation Modelling Practice and Theory 2019, 94:162-176.

[4] X.Zhang,R.-X. Cao. Solar photovoltaic grid power generation and its control inverter. Beijing, China: China Machine Press, 2011, pp. 15-20.

[5] He J,Li Y W,Bosnjak D,et al.Investigation and active damping of multiple resonances in a parallel-inverter-based microgrid[J].IEEE Transaction on power Electronics,2013,28(1):234-246.

[6] Linda Hassaine, Mohamed Rida Bengourina. Control technique for single phase inverter photovoltaic system connected to the grid[J]. Energy Reports,2020,6(Supl.3):200-208.

[7] M.Prodanovic and T. C.Green Control and filter design of three-phase inverters for high power quality grid connection,IEEE Trans. On Power Electronics, 18(2003), No.1, 373-380.